

## Self-consistent energy levels in low-dimensionally delta -doped structures

This article has been downloaded from IOPscience. Please scroll down to see the full text article.

1995 J. Phys.: Condens. Matter 7 731

(<http://iopscience.iop.org/0953-8984/7/4/004>)

View [the table of contents for this issue](#), or go to the [journal homepage](#) for more

Download details:

IP Address: 128.114.163.7

The article was downloaded on 10/07/2012 at 01:41

Please note that [terms and conditions apply](#).

# Self-consistent energy levels in low-dimensionally $\delta$ -doped structures

Y Takagaki and K Ploog

Paul-Drude-Institut für Festkörperelektronik, Hausvogteiplatz 5-7, 10117 Berlin, Germany

Received 22 August 1994, in final form 10 October 1994

**Abstract.** We investigate the electronic states in low-dimensional semiconductor systems created by  $\delta$  doping of donors by solving Schrödinger and Poisson equations self-consistently. The increase of the density of states near the population threshold leads to the existence of two physical solutions to the same boundary-value problem due to the electron-donor dipole charge potential. An empty and a filled state can be self-consistent for a depletion potential in the two-dimensional system for heavy carriers as well as in the one-dimensional and zero-dimensional systems. The bistable behaviour for electrons in the GaAs wire persists up to  $\sim 37$  K if level broadening is negligible. We find that the energy levels of the lowest subband are well described using simple variational functions. The carrier density does not vanish gradually as the doping density that compensates the fixed depletion charge is decreased, indicating that true bistability does not take place in these systems.

## 1. Introduction

The increase of the density of states (DOS)  $g(E)$  at energies  $E$  near the bottom of the transverse subbands,  $g(E) \propto E^{(d-2)/2}$  for  $d = 1, 2,$  and  $3$ , is one of the prominent features of low-dimensional systems and has been anticipated to improve device performance [1, 2]. In optical devices, the energy distribution of the injected carriers is squeezed as the spatial dimensionality  $d$  is reduced, leading to low-threshold and narrow-spectral-width laser operation [1]. In the last decade, semiconductor quantum wires and dots have been fabricated using various techniques, and many novel characteristics have been discovered [3]. In addition, a considerable number of theoretical studies has been devoted to examining the one-dimensional (1D) and zero-dimensional (0D) states in these structures [4–9]. Additional confinements of a two-dimensional (2D) electron gas in heterojunctions, where the large band gap discontinuity provides an almost ideal hard-wall potential in the direction perpendicular to the heterointerface, are very often realized by means of depletion-type techniques [3]. The specific nature of the confined states, thus, depends crucially on the geometrical features of the structures. This fact requires us to solve the Poisson equation self-consistently even in a primitive analysis since screening effects play an essential role in establishing the confining potential in the vicinity of the channel boundary [7]. The self-consistency of the lateral potential depletion has been shown to imply a significant importance in edge-state equilibration [10]. Nixon and Davies [4] employed the Thomas–Fermi model to investigate the disordered potential in 1D channels due to the random distribution of donors in selectively doped heterostructures. Quantum-mechanical calculations of the 1D and 0D subbands were presented, for example, by Laux and Stern [7] and by Kumar and co-workers [9], respectively. The 0D energy levels in quantum dots are directly reflected in the Coulomb-blockade oscillations and have been studied extensively [11, 12]. We emphasize that the

role of the neutral region, which surrounds the depletion region of the quantum structures, was often omitted in the previous studies. Consequently, the position of the Fermi level was determined relative to the quantized energy levels to achieve required carrier densities. In reality, the Fermi level should be determined to be consistent with the whole system.

In this paper, we investigate the electrostatic potential and the electron distribution in low-dimensional structures provided by  $\delta$  doping in GaAs. We explicitly take into account the presence of the neutral region, so that the position of the Fermi energy  $E_F$  is determined *globally*. We have calculated the subband threshold energy as a function of the charge density  $N_d$  in the depletion region. Self-consistent treatment of the Poisson and Schrödinger equations yields two static solutions associated with the subband population. Because of the singular DOS in 1D and 0D systems, a significant number of electrons suddenly occupies the subband at the moment the bottom energy is lowered below  $E_F$ . The threshold energy is pushed down abruptly as a consequence of a large electron-donor dipole potential originating from the excessive electron occupation, resulting in a jump in the threshold energy (and also in the electron density) when  $N_d$  is increased. On the other hand, if the threshold energy is raised from a value for which the subband is originally filled by decreasing  $N_d$ , the subband is depleted at a lower value of  $N_d$  compared to the reverse direction. The electronic states hence exhibit two physical solutions for a range of  $N_d$  around the onset of the population. We also calculate the energy levels using the variational wave-function technique [6, 13] at temperature  $T = 0$  K. We find that this approach confirms excellently the results of the numerical simulation. Since the analysis is completely analytical, detailed physical insight into the nature of the electron states can be provided.

## 2. Low-dimensional $\delta$ -doped structures

In this section, we describe our model structure by considering a quantum wire produced by line doping of Si donors in GaAs [14], which is illustrated in figure 1(a). The cylindrical doped region is assumed to be perfectly straight, so that the electron wave function in the  $z$  direction is represented by plane waves. The charge density in the structure consists of the distributions of free electrons and ionized donors and background acceptors. We assume a uniform distribution of the ionized-donor charge within the radius  $a$ . The background-acceptor density is also assumed to be uniform and equal to  $n_A = 10^{20} \text{ m}^{-3}$ . In searching for a self-consistent solution of the Schrödinger and Poisson equations, we divide the total doping density into two parts [15],  $n_D = n_D^{\text{dpl}} + n_D^{\text{el}}$ . The ionized acceptor charge is compensated by  $n_D^{\text{dpl}}$ , and so  $\pi a^2 n_D^{\text{dpl}} = \pi D^2 n_A \equiv N_d$ , where  $D$  is the radius of the depletion region. The free electrons are generated by  $n_D^{\text{el}}$ , i.e.

$$\int n(r) 2\pi r dr = \pi a^2 n_D^{\text{el}} \equiv N_s. \quad (1)$$

Correspondingly, the Poisson equation is separated as

$$(d^2/dr^2 + (1/r) d/dr) V_d(r) = e^2 [n_D^{\text{dpl}}(r) - n_A(r)]/\epsilon \quad (2a)$$

$$(d^2/dr^2 + (1/r) d/dr) V_s(r) = e^2 [n_D^{\text{el}}(r) - n(r)]/\epsilon \quad (2b)$$

where  $\epsilon$  is the dielectric constant of GaAs. The solution of (2a), i.e., the depletion potential due to the fixed space charge, is

$$V_d(r) = E_A - (e^2 N_d / 4\pi \epsilon) [2 \ln(D/a) - [(D^2 - a^2) / D^2 a^2] r^2] \quad 0 < r < a \quad (3a)$$

$$= E_A - (e^2 N_d / 4\pi \epsilon) [2 \ln(D/r) + (r/D)^2 - 1] \quad a < r < D \quad (3b)$$

$$= E_A \quad D < r. \quad (3c)$$

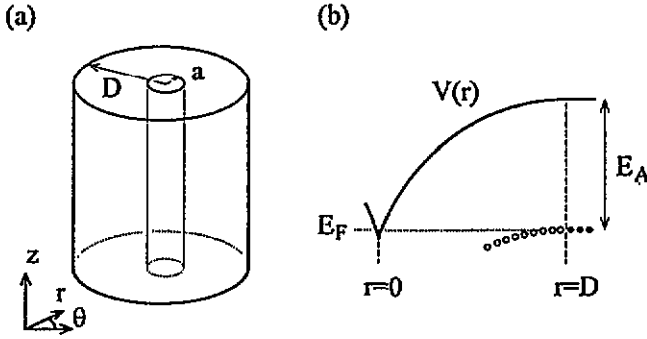


**Figure 1.** (a) A schematic view of a line-doped structure. The dopant atoms are confined in the cylinder of radius  $a$ . The ionized background acceptor charge is distributed uniformly in the depletion region of radius  $D$ . The depletion region is surrounded by a neutral region. (b) The profile of the conduction band edge  $V(r)$  in the radial direction. The Fermi level  $E_F$  is fixed at the acceptor level  $E_A$  in the neutral region. The open and filled circles represent ionized and neutral acceptors, respectively.

We consider that the system is in equilibrium, so that the Fermi level  $E_F$  in the neutral region is fixed, at  $T = 0$  K, at the acceptor level  $E_A$  (see figure 1(b)). When  $E_F$  lies above  $E_A$ , the acceptor impurities are fully ionized. Throughout this article, all energies are measured relative to the Fermi level, i.e.,  $E_F$  is set to be zero. For simplicity, we assume that  $E_A$  is located at the midgap of GaAs. The results to be shown below do not depend qualitatively on the value of  $E_A$ . The electron density  $n(r) = \sum N_i |\varphi_i(r)|^2$  is obtained through the solution of the Schrödinger equation. Here, the sum runs over the occupied 1D modes and the linear electron density  $N_i$  of the  $i$ th mode with the threshold energy  $E_i$  is

$$N_i = (1/\pi)(2mk_B T/\hbar^2)^{1/2} F_{-1/2}((E_F - E_i)/k_B T) \tag{4}$$

where  $F_k$  is the Fermi–Dirac integral of order  $k$  and  $m$  is the effective mass of electrons in GaAs. Because of the cylindrical symmetry, the wave function is separable in radial and angular directions:

$$\Psi_{n,l}(r, \theta) = [\varphi_{n,l}(r)/\sqrt{2\pi}] e^{il\theta} \quad l = 0, 1, 2, \dots \tag{5}$$

where  $\varphi_{n,l}(r)$  satisfies the radial equation

$$(1/r)((d/dr)(r d\varphi_{n,l}(r)/dr)) + [(2m/\hbar^2)\{E_{n,l} - V(r)\} - l^2/r^2]\varphi_{n,l}(r) = 0$$

$$n = 1, 2, 3, \dots \tag{6}$$

The total (effective) energy of the conduction band edge is given as

$$V(r) = V_d(r) + V_s(r) + V_{xc}[n(r); r]. \tag{7}$$

We include many-body effects in the numerical calculation. The exchange–correlation potential  $V_{xc}$  is evaluated within the local-density approximation [16]:

$$V_{xc}[n(r); r] = -(e^2/8\pi\epsilon a_0)(2/\pi\alpha r_s)[1 + 0.0545r_s \ln(1 + 11.4/r_s)] \tag{8}$$

where  $\alpha = (4/9\pi)^{1/3}$ ,  $r_s = [4\pi a_0^3 n(r)/3]^{-1/3}$ , and  $a_0 = 4\pi\epsilon\hbar^2/me^2$  is the effective Bohr radius.

### 3. Numerical solutions

In this section, we solve (2b) and (6) numerically for a given  $n_D^{\text{dpl}}$ . The analytical approach using a variational function is discussed in the next section. Since the Fermi level is initially fixed in our approach, the total doping density is determined to satisfy charge neutrality,  $N_s = \sum N_i$ . The presence of the electrons increases the separation of the conduction-band edge from the Fermi level. One may hence suspect that the iteration can diverge. We have found, however, that the convergence is achieved rapidly without using the damping factor [17], which is often introduced to stabilize the simulation.

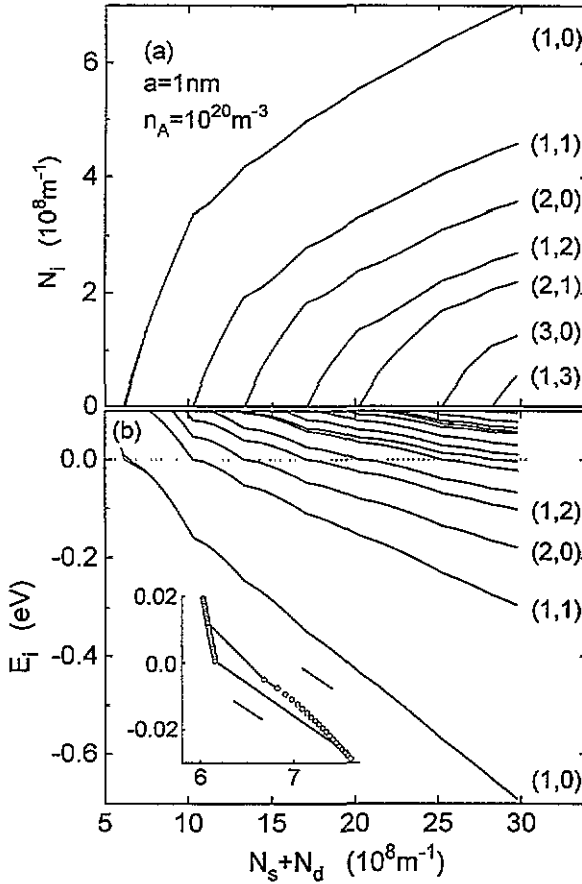


**Figure 2.** (a) The linear electron density  $N_i$  and (b) the threshold energy  $E_i$  of modes  $i = (n, l)$  as a function of the total linear doping density  $N_s + N_d$  at  $T = 0$  K. In (b) the Fermi level, which is set to be zero, is indicated by the dotted line. The hysteresis in  $E_{1,0}$  around the population threshold is expanded in the inset. The arrows indicate the direction of the variation of the doping density.

The linear electron density  $N_i$  and the threshold energy  $E_i$  of 1D modes  $i = (n, l)$  are shown in figure 2 as a function of the total linear doping density for  $T = 0$  K. Because of the singular 1D DOS, a significant number of electrons populate the modes even when the threshold energy is only slightly below  $E_F$ . As has been observed in the 2D case [13],

the Fermi energy is pinned at the bottom of the 1D modes when it crosses the threshold energies, resulting in the discontinuous increase of  $N_i$ . One finds a hysteresis accompanying the population of each mode as the doping density is varied. In solving the equations for a series of  $N_d$ , the previous solution is used as an initial guess in the iteration for self-consistency. The hysteresis in  $E_{1,0}$  is expanded in the inset of figure 2(b).

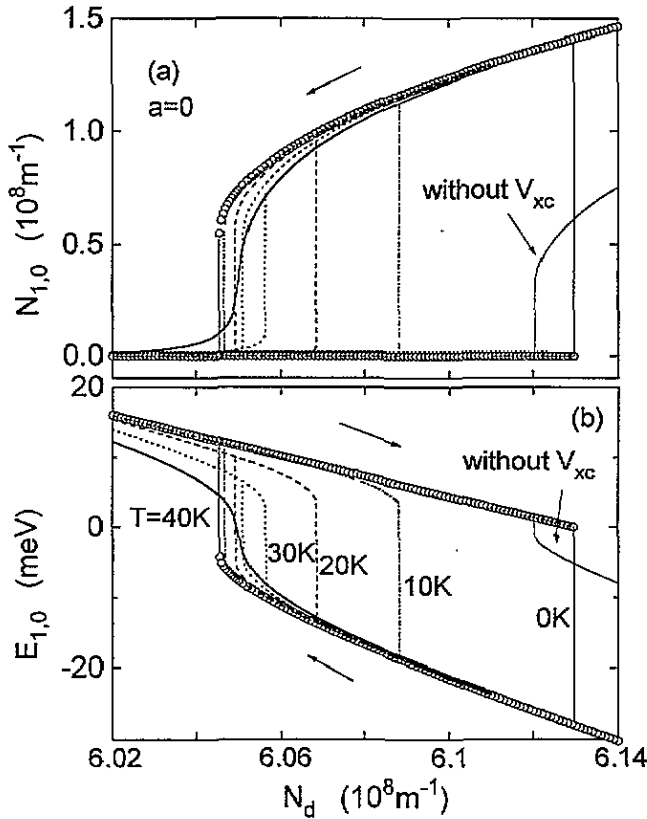


Figure 3. (a) The linear electron density  $N_{1,0}$  and (b) the threshold energy  $E_{1,0}$  of the lowest mode as a function of  $N_d$  calculated at  $T = 0$  (thin solid line and circles), 10 (dash-dotted line), 20 (dashed line), 30 (dotted line), and 40 K (solid line). Ideal  $\delta$ -function-type doping ( $a = 0$ ) is assumed. The bistability disappears for  $T > 37$  K. Results within the Hartree approximation, which exhibit smaller hysteresis, are also shown for  $T = 0$  K. The arrows indicate the direction of the variation of  $N_d$ .

In figure 3, we show the electron density  $N_{1,0}$  and the threshold energy  $E_{1,0}$  of the lowest mode as a function of  $N_d$ . We have assumed here an ideal  $\delta$ -function-type donor distribution (i.e.,  $a = 0$ ). This variation of  $a$  makes no practical difference except an overall shift in the doping density, though the hysteresis becomes smaller as  $a$  is increased beyond the extension of the electron wave function. The hysteresis is better illustrated here since  $N_d$  is roughly unchanged in figure 2 once the modes are occupied. At  $T = 0$  K, modes are populated by electrons when the threshold energy crosses  $E_F$  as  $N_d$  is increased. Just after the level crossing at  $N_d = N_d^U$ , a considerable number of electrons suddenly occupy the mode because of the singular 1D DOS. As we are dealing with the  $\delta$ -doped

system, this corresponds to a creation of an electron-donor dipole charge in addition to the fixed space charge. The conduction-band edge, and consequently the threshold energy, is substantially lowered due to the dipole-charge potential  $V_s$ , leading to the abrupt jump in  $N_{1,0}(E_{1,0})$  to  $N_{1,0}^U(E_{1,0}^U)$ . Note that the energy level is pushed up if only electrons are added to the channel, i.e., the dipole charge in the  $\delta$ -doped system is essential for the hysteresis effect. On the other hand, when  $N_d$  is decreased from a value for which the mode is initially populated,  $N_{1,0}$  remains finite and decreases gradually even for  $N_d < N_d^U$  due to the space charge stored in the cylindrical well. Eventually, the mode is depleted at  $N_d = N_d^L < N_d^U$ . Therefore, the self-consistent potential exhibits two solutions for the doping densities of  $N_d^L < N_d < N_d^U$  as shown in figure 4. It should be noted that the total doping densities corresponding to the two electron states shown in figure 4 are different, i.e.,  $N_d$  for the empty state and  $N_d + N_s$  for the filled state. Nonetheless, our result demonstrates that two distinct electron states can be self-consistent with a certain depletion potential in low-dimensional systems. The exchange–correlation effect, which is usually not very important in GaAs, enhances the hysteresis effect drastically, as shown in figure 3 for  $T = 0$  K, since we are dealing with a regime of low electron concentration where the average kinetic energy of electrons is comparable to the average interaction energy [13]. We note, however, that the effect is not essential for the occurrence of the bistable behaviour itself. In double-barrier resonant-tunnelling semiconductor heterostructures, bistability due to the build-up of negative space charge in the quantum well between the two barriers has been observed in the current–voltage characteristics [18]. We emphasize that the resonant tunnelling represents a dynamical process, while the effect presented here is due to a static charge build-up. The singular DOS belonging to the mode that crosses  $E_F$  is responsible for the abrupt jump in the level energy, so that hysteresis takes place also when multiple modes are occupied. However, the hysteresis becomes smaller for higher modes since the addition of more electrons to the lower modes effectively weakens the singularity. In figure 2, the hysteresis for higher modes is nearly invisible since the charge accumulation into the lower modes dominates the change of the total doping density.

If  $N_{1,0}$  continuously approaches zero as  $N_d$  decreases, the energy level possesses true bistability. However, our numerical simulation indicates that this is not the case. On the contrary, there is a finite range of the total doping density,  $N_d^L < \pi a^2 n_D < N_d^L + N_{1,0}^L$ , for which our scheme does not give a solution since  $N_{1,0}^L > N_d^U - N_d^L$  in our model structure. If  $n_D$  is fixed, as is the case in conventional simulations [7, 9],  $N_s$  will be able to take arbitrary values around zero. However, these states are not ‘stable’ in our approach.

In the classical approximation, the local electron density is estimated using the three-dimensional DOS and the Fermi–Dirac statistics [4, 5]. Hysteresis is found not to take place in the classical simulation because of the slow increase of the number of electrons [15]. We have applied our numerical technique to a conventional 2D  $\delta$ -doped structure and found that the bistability does not take place either (for electrons). Broadening of energy levels due to scattering and thermal spread of the Fermi distribution smear out the singularity of the 1D DOS. The results of a simulation at several temperatures are shown in figure 3. At finite temperatures, the Fermi level in the neutral region needs to be adjusted to balance the ionizations of the background donors and acceptors. We have assumed, however, that  $E_F$  is always fixed at  $E_A$ . This simplification will be reasonable at the low temperatures considered here. The excited states are substantially above  $E_F$  in the regime of the hysteresis, and so the temperature effect primarily arises from the thermal population of the lowest mode. Although the abrupt jump in  $E_{1,0}$  is triggered at lower  $N_d^U$  with increasing  $T$ , it is still present over a wide range of  $T$ , indicating that the effect can survive in the presence of moderate disorder. The hysteresis disappears at  $T_c \sim 37$  K as the thermal energy becomes

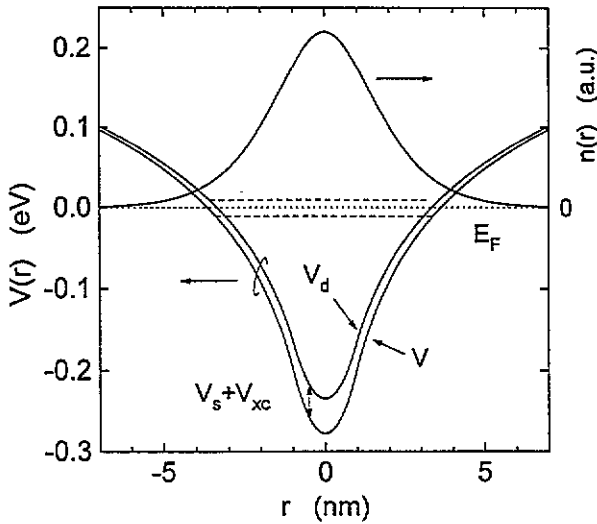


**Figure 4.** Two solutions of the effective potential  $V(r)$  and the electron distribution  $n(r)$  when the mode is occupied ( $N_{1,0} = 8.8 \times 10^7 \text{ m}^{-1}$ ) for  $a = 1 \text{ nm}$  and  $N_d = 6.1 \times 10^8 \text{ m}^{-1}$  at  $T = 0 \text{ K}$ . The dashed lines indicate the corresponding mode threshold energies (9.3 and  $-10.9 \text{ meV}$ ). The dotted line represents the Fermi level  $E_F$ . When the mode is not occupied,  $V = V_d$ .

comparable to the separation of the two stable branches in  $E_{1,0}$ . We have also examined the hysteresis effect when the effective mass of the carriers is increased to simulate heavy holes, where we obtain  $N_d^U - N_d^L = 3.1 \times 10^7 \text{ m}^{-1}$ ,  $E_{1,0}^U = 126 \text{ meV}$ ,  $N_{1,0}^U = 8.4 \times 10^8 \text{ m}^{-1}$ , and  $T_c \sim 170 \text{ K}$ . The bisolution behaviour is enhanced for heavier carriers due to stronger many-body effects [13] and confinement of the carriers near the parent dopant atoms [15]. However, the level broadening, which is not included in the simulation, will be critical in the p-type channel.

#### 4. The variational wave-function approach

We now investigate the electronic states in the 2D, 1D and 0D  $\delta$ -doped structures using the variational wave-function technique [13]. We neglect the many-body exchange–correlation effects, for simplicity. The Hartree approximation may not be appropriate to examine the behaviour in the low-electron-density limit, as evidenced by the numerical simulation in the previous section. However, we think that the qualitative trend of the bisolution behaviour can be described within our approximation.

Let us first consider the line-doped quantum wire. We assume that the donor atoms are confined in a cylinder of infinitesimal radius. The potential energy  $V_s(r)$  due to free carriers induced in the space-charge region is given by the solution of the Poisson equation with the electron charge density and the corresponding donor density as the source term:

$$\rho_s(r) = -eN_s^{1D}[|\varphi(r)|^2 - \delta(r)] \tag{9}$$

and so

$$V_s(r) = -\frac{e^2 N_s^{1D}}{\epsilon} \int_{-\infty}^r \frac{dr'}{r'} \int_{-\infty}^{r'} r'' |\varphi(r'')|^2 dr'' \tag{10}$$



We employ the following variational wave-function for the lowest subband [13]:

$$\varphi_0(r) = (2/\pi)^{1/2} b e^{-br}. \quad (11)$$

The average radius  $r_0 \equiv \langle r \rangle$  of the electron channel for this wave function is  $b^{-1}$ . Because of the simplicity of the wave function, the expectation values of all the energy terms in the Hamiltonian are easily evaluated. The expectation values of the kinetic energy  $T$ ,  $V_d$ , and  $V_s$  are given by

$$\langle T \rangle = \hbar^2 \beta^2 / 8mD^2 \quad (12)$$

$$\langle V_d \rangle = E_A + (e^2 N_d^{1D} / 4\pi\epsilon)(3 - 2C - 2 \ln \beta - 6/\beta^2) \quad (13)$$

$$\langle V_s \rangle = \alpha e^2 N_s^{1D} / \pi\epsilon \quad (14)$$

where  $D = (N_d^{1D} / \pi n_A)^{1/2}$ ,  $\alpha = (\ln 2) / 2 - \frac{1}{8}$ , and  $C = 0.577$  is the Euler constant [19]. In (13), we have assumed that  $\beta \equiv 2bD \gg 1$ . The ground electronic state is obtained by minimizing the total energy per electron,  $\langle T \rangle + \langle V_d \rangle + \frac{1}{2} \langle V_s \rangle$ , where the factor  $\frac{1}{2}$  in the last term prevents double counting of electron–electron interactions. Since  $\langle V_s \rangle$  does not explicitly depend on  $\beta$ , the energy minimization can be made independent of  $N_s$ . This is a great advantage of the 1D case since  $N_s^{1D}$  needs to be determined to satisfy self-consistency. If we omit the  $\beta^{-2}$  term in (13), the value of  $\beta$  to minimize the total energy per electron is given by

$$\beta_0 = 2D/r_0 = 2D(2N_d^{1D}/a_0)^{1/2}. \quad (15)$$

The threshold energy of the lowest subband is

$$\begin{aligned} E_0^{1D} &= \langle T \rangle + \langle V_d \rangle + \langle V_s \rangle = E_A + \frac{e^2 N_d^{1D}}{4\pi\epsilon} \left[ 4 - 2C - \ln \left( \frac{8D^2 N_d^{1D}}{a_0} \right) \right] - \frac{\alpha e^2 N_s^{1D}}{\pi\epsilon} \\ &= V_0 - \frac{\alpha e^2 N_s^{1D}}{\pi\epsilon} \end{aligned} \quad (16)$$

where  $V_0$  is the threshold energy when  $N_s^{1D} = 0$ . If the subband is occupied below  $E_F$ ,  $N_s^{1D}$  needs to satisfy the self-consistency condition. The linear electron density in (14) is related to the energy difference  $|\langle V_s \rangle| - V_0$  between the Fermi level and the subband threshold (when  $|\langle V_s \rangle| \geq V_0 \geq 0$ ) through the 1D DOS. Therefore, we obtain

$$|\langle V_s \rangle| = \alpha e^2 N_s^{1D} / \pi\epsilon = (16\alpha \text{Ry}^{1/2} / \pi\epsilon) (|\langle V_s \rangle| - V_0)^{1/2} \quad (17)$$

where  $\text{Ry} = me^4 / 32\pi^2 e^2 \hbar^2$  is the effective Rydberg. We find

$$|\langle V_s \rangle| = (128\alpha^2 / \pi^2) \text{Ry} + [((128\alpha^2 / \pi^2) \text{Ry})^2 - (256\alpha^2 / \pi^2) \text{Ry} V_0]^{1/2}. \quad (18)$$

The results are plotted in figure 5. If the threshold energy is plotted as a function of  $N_d^{1D}$ , one finds two solutions for  $0 \leq V_0 \leq 64(\alpha/\pi)^2 \text{Ry}$ . When  $V_0 \rightarrow 0+$ ,  $E_0^{1D}$  jumps from zero to  $-256(\alpha/\pi)^2 \text{Ry}$ . On the other hand, the threshold energy is  $-64(\alpha/\pi)^2 \text{Ry} < E_0^{1D} < -256(\alpha/\pi)^2 \text{Ry}$  when  $N_d^{1D}$  is decreased from a value for which the subband is originally occupied. However,  $E_0^{1D}$  does not approach zero gradually but jumps from  $-64(\alpha/\pi)^2 \text{Ry}$  to  $64(\alpha/\pi)^2 \text{Ry}$  when  $V_0 = 64(\alpha/\pi)^2 \text{Ry}$ . This instability in the low

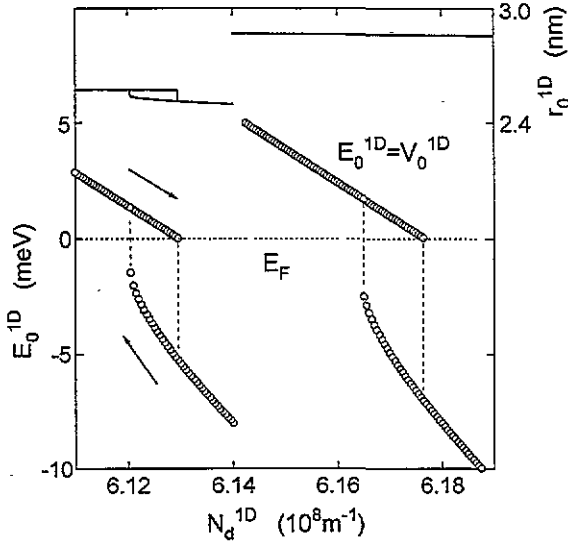


**Figure 5.** The bottom energy of the lowest subband  $E_0^{1D}$  and the average radius of the wave function  $r_0^{1D}$  in a 1D  $\delta$ -doped quantum wire. The results of the numerical simulation in the Hartree approximation are shown at  $N_d^{1D} = 6.11\text{--}6.14 \times 10^8 \text{ m}^{-1}$ , while those of the analytical approach are shown at  $N_d^{1D} = 6.14\text{--}6.19 \times 10^8 \text{ m}^{-1}$ . The arrows indicate the direction of the variation of  $N_d^{1D}$ .

carrier density is in agreement with the numerical result. The minimum electron density given by  $16\alpha/\pi^2 a_0$  is  $3.6 \times 10^7 \text{ m}^{-1}$  in GaAs and is much larger than the change of  $N_d^{1D}$  in the regime of bistolution behaviour. Consequently, the 1D system does not exhibit bistability if the subband energy is displayed as a function of the total doping density  $N_d^{1D} + N_s^{1D}$ . The bistolution behaviour is stronger in semiconductors with a larger effective mass and a smaller dielectric constant, such as Si. We note that  $r_0$  is solely determined by  $N_d^{1D}$  when the variational function (11) is used. Our numerical simulation, however, indicates that  $r_0$  depends on the electron density and takes two different values corresponding to the two solutions.

We have applied a similar procedure to a 2D  $\delta$ -doped system with infinitesimal thickness of the doped plane. If we assume the  $e^{-b|z|}$ -type variational wave function [20] (the  $z$  direction is perpendicular to the doped plane), we have, instead of (13) and (14),

$$\langle V_d \rangle = E_A - (e^2 N_d^{2D} D / 2\epsilon) (\frac{1}{2} - 1/\beta + 1/\beta^2) \tag{19}$$

$$\langle V_s \rangle = (e^2 N_s^{2D} D / 4\epsilon) / \beta \tag{20}$$

where  $N_d^{2D}$  and  $N_s^{2D}$  are the corresponding sheet-doping densities, and the depletion width is given by  $D = N_d^{2D} / 2n_A$ . We have chosen the constant of integration to make  $V_s(0) = 0$ , and so  $V_s(z) \rightarrow e^2 N_s^{2D} D / 2\epsilon\beta$  when  $z \rightarrow \infty$  [13]. This offset is to be subtracted when we calculate the subband energy. The ground-state energy is minimized when  $\beta = (8\pi N/a_0)^{1/3} D$  with  $N = N_d^{2D} + \frac{1}{4} N_s^{2D}$  if only the  $\beta^{-1}$  term in (19) is retained. The subband energy is thus given by

$$E_0^{2D} = E_A - e^2 N_d^{2D} D / 4\epsilon + (\hbar^2 e^4 / 2m\epsilon^2)^{1/3} (N^{2/3} / 4 + N_d^{2D} / 2N^{1/3} - N_s^{2D} / 4N^{1/3}). \tag{21}$$

The self-consistent condition,  $N_s^{2D} = (m/\pi\hbar^2)|E_0|$ , is now given by

$$3 + n(1 + n/4)^{-1/3} - (1 + n/4)^{2/3} - 2(1 + n/4)^{-1/3} = \gamma(n - m|V_0|/\pi\hbar^2 N_d^{2D}) \quad (22)$$

where  $n = N_s^{2D}/N_d^{2D}$ ,  $\gamma = \gamma_0(\pi a_0^2 N_d^{2D})^{1/3}$  with  $\gamma_0 = 2$ , and  $V_0$  is the subband energy when  $N_s^{2D} = 0$ . One finds that the bisolution behaviour does not take place in the 2D system when  $\gamma > 1$ , and

$$|E_0| = (1 - \gamma^{-1})^{-1} |V_0| \quad (23)$$

in the limit of  $N_s^{2D} \ll N_d^{2D}$ . When  $\gamma$  is reduced to unity, the slope of  $|E_0|$  with respect to  $|V_0|$  becomes infinity, suggesting the occurrence of bistability. The numerical calculation shown in figure 6 indicates that this is indeed the case. Since the 2D DOS is proportional to the effective mass, the hysteresis effect emerges, according to our numerical simulation, when the effective mass is larger than  $\sim 0.15m_0$  (corresponding to  $\gamma_0 = 2.8$ ) for GaAs in the Hartree approximation [20]. Therefore, n-type  $\delta$ -doped GaAs will show normal behaviour, whereas the hysteresis effect is anticipated for heavy holes provided level broadening is negligible.

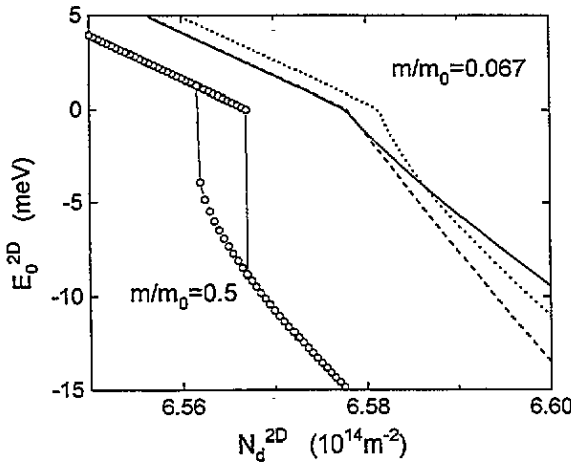


Figure 6. The bottom energy of the lowest subband in a 2D  $\delta$ -doped quantum well. Solid lines and circles show results of numerical simulations in the Hartree approximation for the effective masses of  $0.5m_0$  and  $0.067m_0$ . Analytical results using trial functions  $b^{1/2} \exp(-b|z|)$  and  $(2b/5)^{1/2} (b|z| + 1) \exp(-b|z|)$  are shown by dotted and dashed lines, respectively.

Let us finally consider an ideal 0D  $\delta$ -doped system, which is similar to the H atom [21]. In a 0D system, the total electron charge can be only integer multiples of  $e$ , and so the hysteresis effect is expected to be significant. In quantum dots, spin degeneracy is broken due to Coulomb blockade [22]. However, we neglect the spin splitting, for simplicity. The expectation values of  $V_d$  (in the limit of  $\beta \gg 1$ ) and  $V_s$ , when a trial function  $(b^3/\pi)^{1/2} e^{-br}$  is used, are given by

$$\langle V_d \rangle = E_A + (e^2 N_d^{0D} / 8\pi \epsilon D) (3 - \beta - 12/\beta^2) \quad (24)$$

$$\langle V_s \rangle = -(3e^2 N_s^{0D} / 64\pi \epsilon D) \beta \quad (25)$$

where  $N_d^{0D}$  and  $N_s^{0D}$  are the numbers of donors, and the radius of the depletion region is  $D = (3N_d^{0D}/4\pi n_A)^{1/3}$ . Keeping only the leading term in  $\langle V_d \rangle$ , the lowest discrete energy level is given by

$$E_0^{0D} = E_A + 3e^2 N_d^{0D} / 8\pi \epsilon D - (N_d^{0D} + \frac{3}{16} N_s^{0D})(N_d^{0D} + \frac{9}{16} N_s^{0D}) Ry. \quad (26)$$

The magnitude of  $\langle V_s \rangle$  is given by

$$|\langle V_s \rangle| = \frac{3}{4} [N_d^{0D} + \frac{3}{16} N_s^{0D}] N_s^{0D} Ry. \quad (27)$$

Although  $\langle V_s \rangle$  depends on  $\beta$ , the lowest energy level can accommodate only two electrons, i.e.,  $N_s^{0D}$  is either zero or two. Therefore, we can deduce the energy shift due to the level occupation if we ignore possible population of excited energy levels. The dependence of  $E_0^{0D}$  on  $N_d^{0D}$  is shown in figure 7. Here,  $N_d^{0D}$  is treated as a continuous variable for convenience. We have also evaluated the energy of excited levels [21] numerically. The second-level energy is  $> 0.57$  eV for the doping densities in figure 7, so that the effects of higher levels are negligible where the hysteresis of the lowest level is concerned. The energy separation between the two branches in  $E_0$  is drastically increased on reducing the dimensionality. Although  $E_0^{0D}$  gradually approaches zero, one finds that the electron state when 12 ionized donors are embedded is not stable in our approach because of the discreteness of the electron charge stored in the level.

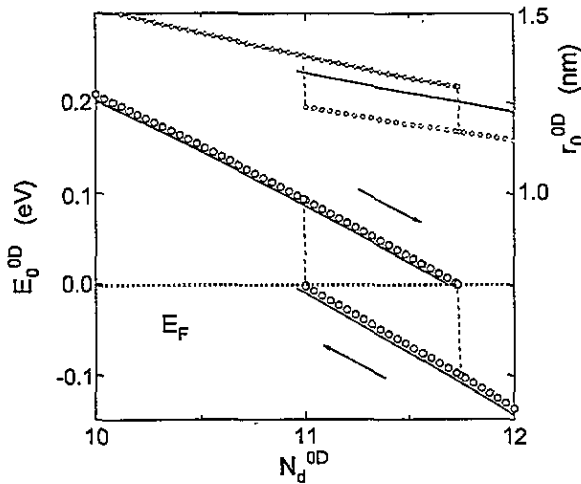


Figure 7. The lowest energy level  $E_0^{0D}$  and the average radius of the wave function  $r_0^{0D}$  in a 0D  $\delta$ -doped quantum dot in the Hartree approximation. The analytical results are shown by solid lines whereas the numerical ones are shown by circles. Two electrons are accommodated for the filled state. The excited energy levels appear far above this energy range ( $> 0.57$  eV). The arrows indicate the direction of the variation of  $N_d^{0D}$ , which is regarded as a continuous variable.

## 5. Summary

In conclusion, we have demonstrated that the self-consistent energy levels in low-dimensionally  $\delta$ -doped structures can possess two solutions associated with the onset of the mode population. This effect originates from the excessive carrier occupation due to the singular DOS. The large electron-donor dipole charge potential abruptly pushes down the energy level. We point out that it is important to separate the donor density into two parts,  $N_s$  and  $N_d$ . The hysteresis effect may be obscured if only the total doping density is considered. We have developed the variational wave function technique in the Hartree approximation to examine the nature of the hysteresis effect. The use of a variational function means that only an upper bound to the true ground-state energy is obtained. However, the energy gap between the two branches is found to be in good agreement with the numerical calculations, indicating that the simple trial functions we used reasonably resemble the true wave functions. Our result indicates an existence of critical mass in the 2D case. Our observation provides a possibility that hysteresis occurs in the energy levels in low-dimensional systems beginning to fill with electrons, or empty. If the filled-state energy level in a 1D system reaches the Fermi level continuously as the doping density is reduced, the system shows true bistability. However, because of the level instability at low carrier densities, the electronic states do not exhibit true bistability in the structures considered in this article. One needs alternative structures or material systems to overcome this instability. Further investigation to understand the mechanism of the instability is also required. Unfortunately, the electron mobility in a  $\delta$ -doped system is typically low due to the large overlap of the electron wave function and the parent ionized impurities. Therefore, the bistability effect found here may not survive in real samples. However, if one could construct, for example, a structure in which an AlGaAs column with doping along the centre is embedded in GaAs, the selective doping would improve the mobility and reduce the level broadening due to random distribution of impurities. We note that the energy separation between the two branches associated with the bistability becomes larger in lower-dimensional systems, so the disorder effect may not be critical in a 0D system. If the Coulomb-potential effect associated with filling and emptying the state has a significant importance, it is most likely to show up in the experiments in a 0D system.

## Acknowledgments

The authors would like to thank M Wassermeier and H Grahn for a critical reading of the manuscript. This work was supported in part by the Bundesministerium für Forschung und Technologie of Germany.

## References

- [1] Arakawa Y and Sakaki H 1982 *Appl. Phys. Lett.* **40** 939
- [2] Yamada T and Sone J 1989 *Phys. Rev. B* **40** 6265
- [3] For a review, see Beenakker C W J and van Houten H 1991 *Solid State Physics* vol 44, ed H Ehrenreich and D Turnbull (San Diego: Academic) p 1
- [4] Nixon J A and Davies J H 1990 *Phys. Rev. B* **41** 7929
- [5] Luscombe J H and Luban M 1990 *Appl. Phys. Lett.* **57** 61
- [6] Lai W Y and Das Sarma S 1986 *Phys. Rev. B* **33** 8874
- [7] Laux S E and Stern F 1986 *Appl. Phys. Lett.* **49** 91
- [8] Sun Y and Kirczenow G 1993 *Phys. Rev. B* **47** 4413

- [9] Kumar A, Laux S E and Stern F 1990 *Phys. Rev. B* **42** 5166
- [10] Chklovskii D B, Shklovskii B I and Glazman L I 1992 *Phys. Rev. B* **46** 4026
- [11] Beenakker C W J, van Houten H and Staring A A M 1991 *Granular Nanoelectronics* ed D K Ferry, J R Baker and C Jacoboni (New York: Plenum) p 359; 1991 *Phys. Rev. B* **44** 1657
- [12] McEuen P L, Foxman E B, Meirav U, Kastner M A, Meir Y, Wingreen N S and Wind S J 1991 *Phys. Rev. Lett.* **66** 1926
- Stopa M 1993 *Phys. Rev. B* **48** 18340
- [13] Ando T, Fowler A B and Stern F 1982 *Rev. Mod. Phys.* **54** 437
- [14] Bauer G E W and Van Gorkum A A 1990 *Science and Engineering of One- and Zero-Dimensional Semiconductors* ed S E Beaumont and C M Sotomayor Torres (New York: Plenum) p 133
- Wood C E C 1992 *J. Appl. Phys.* **71** 1760
- Däweritz L, Hagenstein K and Schützendübe P 1993 *J. Vac. Sci. Technol. A* **11** 1802
- [15] Takagaki Y, Friedland K J and Ploog K 1994 *Appl. Phys. Lett.* **64** 3258
- [16] Hedin L and Lundqvist B I 1971 *J. Phys. C: Solid State Phys.* **4** 2064
- [17] Stern F 1970 *J. Comput. Phys.* **6** 56
- [18] Goldman V J, Tsui D C and Cunningham J E 1987 *Phys. Rev. Lett.* **58** 1256
- Sheard F W and Toombs G A 1988 *Appl. Phys. Lett.* **52** 1228
- [19] Bronstein I N and Semendjajew K A 1979 *Taschenbuch der Mathematik* (Frankfurt: Harri)
- [20] The trial function has a discontinuous gradient at  $z = 0$ , where the potential energy does not diverge in the 2D case. We have also used a function  $(2b/5)^{1/2}(b|z| + 1) \exp(-b|z|)$ . We obtain the same result except for a difference of prefactors, which gives a better agreement with the numerical results as shown in figure 2. For this function, we find  $\gamma_0 = 2.576$ .
- [21] Schiff L I 1968 *Quantum Mechanics* (Tokyo: McGraw-Hill)
- [22] Beenakker C W J 1991 *Phys. Rev. B* **44** 1646